On X-Ray Diffraction Study of Microstructure of ZnO Thin Nanocrystalline Films with Strong Preferred Grain Orientation

R. KUŽEL, J. ČÍŽEK, and M. NOVOTNÝ

Textures, stresses, and strains, as well as the overall so-called real structure, are crucial for properties of thin films deposited by different methods and can have both positive and negative effects depending on the film and its application. They were studied by a combination of different X-ray diffraction (XRD) techniques for several ZnO films. The films prepared by pulsed laser deposition (PLD) on MgO and sapphire single-crystalline substrates and amorphous-fused silica showed different kinds of strong preferred orientation and also different stresses that could be estimated only from the analysis of quite narrow, nonzero intensity regions of diffraction spots. XRD line broadening was analyzed by a combination of different asymmetric scans. Fiber (0001) texture and tensile residual stresses were found on fused silica, while domains with local epitaxy and huge compressive stress were detected on MgO substrate, and surprisingly, very strong local epitaxy but not parallel to the (0001) sapphire substrate was observed. No residual stress was detected there. Some methodological aspects of the XRD studies of thin nanocrystalline films with strong preferred orientation are discussed.

DOI: 10.1007/s11661-012-1432-x

I. INTRODUCTION

ZnO is an attractive material with potential use in ultraviolet optoelectronic devices due to its remarkable properties, such as a direct wide band gap of 3.37 eV or an exciton binding energy of 60 meV at room temperature. ZnO material has found applications in spintronics, gas, and surface acoustic wave sensors and transparent electronics.[1–6] Ultrathin ZnO films are becoming increasingly considered for nanotechnology applications, and they receive considerable attention because of the device potential involving quantum confinement effects, in particular.[7] Ultrathin, uniform ZnO films of nanometer-order thickness can be fabricated by several techniques, *e.g.*, dip coating, sol-gel, magnetron sputtering, or pulsed laser deposition (PLD[8]) as in our case. At ambient conditions, the thermodynamically stable phase of ZnO is wurtzite, hexagonal structure, space group $P6_3mc$.

The microstructural properties of these films, such as preferred orientation, residual stresses, microstrains, and densities of the lattice defects, are of high interest. They can be studied by different microscopic techniques, but X-ray diffraction (XRD) is also very suitable since it can give rich information on the microstructure. It has become a standard in routine phase and structural analysis of thin films.[9] However, routine XRD analysis of polycrystalline or nanocrystalline thin films is not always sufficient for appropriate characterization of particular thin film, and for discovering of all the important features, more detailed studies are required. A problem is that routine XRD scans of thin films where the stresses and preferred orientation can play an important role may lead to missing of the important features, sometimes even substantial for the structure and properties of a particular sample.

Optimum grain size and orientation control, and film performance optimization, is achieved through manipulation of both the conditions of film deposition and postdeposition processing.[10,11] However, especially for very thin films, the substrate type, structure, and microstructure can play an important role for the evolution of texture and stresses. Therefore, the thin film structure and microstructure may be influenced by a number of different parameters (see for example, the monographies in References 12 through 14).

In this article, dependence of microstructure of ZnO films on the type of substrate is studied. Conventional and routine methods of XRD characterization of polycrystalline thin films are summarized first and then applied to the analysis of three ZnO thin films deposited on three different substrates: (100) MgO, (0001) sapphire, and amorphous fused silica (FS). These substrates were selected because of their different crystal structure. They can also be important for the practical applications of the films. The films of the thickness below 100 nm were prepared since up to now most of the studied ZnO films were of higher thickness, and new applications of these films required the wavelengths significantly lower than that of visible light.[7] In this

R. KUŽEL, Associate Professor, is with the Department of Condensed Matter Physics, Faculty of Mathematics and Physics, Charles University, 121 16 Prague 2, Czech Republic. Contact e-mail: kuzel@karlov.mff.cuni.cz J. ČÍŽEK, Associate Professor, is with the Department of Low Temperature Physics, Faculty of Mathematics and Physics, Charles University. M. NOVOTNÝ, Associated Scientist, is with the Department of Analysis of Functional Materials, Institute of Physics, Academy of Sciences of the Czech Republic, Na Slovance 2, 182 21 Prague 2, Czech Republic.

Manuscript submitted April 16, 2012.
Article published online October 2, 2012

case, the role of the substrate becomes more important. This can highly influence thin film preferred orientation and morphology.[9,15] The decrease of the film thickness and/or crystallite size may result in increase of the band gap energy due to the quantum confinement effect.[7,16]

The films have been studied in Reference 17 by a combination of scanning electron microscopy (SEM), slow positron implantation spectroscopy (SPIS), X-ray diffraction, and optical measurements of transmittance and reflectance. It was shown that the substrate plays a negligible role on the optical properties for ZnO films on MgO and FS substrates. Depth-resolved studies by SPIS revealed that the films exhibited a higher concentration of open volume defects than a bulk ZnO single crystal and that the films deposited on single-crystalline substrates contains higher concentration of defects than the film deposited on amorphous FS.

It appeared that a more detailed XRD measurement was desirable and necessary. More details of these studies are presented and discussed in this article.

II. ROUTINE X-RAY MEASUREMENT OF POLYCRYSTALLINE THIN FILMS

Since the SEM pictures[17] showed clearly nanocrystalline microstructure of all the measured deposited films, standard XRD techniques for thin polycrystalline thin films were applied first. Of course, this is rather arbitrary label what techniques are "standard" or "routine." Therefore, they are briefly described for usual setups with point detectors.

A. *Bragg–Brentano Parafocusing Geometry, Symmetric θ–2θ Scan*

Conventional powder diffraction patterns in reflection are usually measured in the Bragg–Brentano (BB) parafocusing geometry by symmetric θ–2θ scan. This scan can also be taken with the parallel beam optics; however, the former method gives significantly better resolution unless a special optics is used in the latter case. In the symmetric scan the information contained in each diffraction line is related to the grains oriented with the corresponding planes parallel to the surface.*

*This is even more strictly fulfilled for the parallel beam while in the parafocusing geometry instrumental aberrations result in nonzero contributions also from slightly inclined planes.

Consequently, the texture-preferred grain orientation can often be quickly estimated and semiquantitatively characterized for example by the so-called Harris texture indices based on the comparison of the experimental intensities with the corresponding theoretical intensities for powder. However, this is only possible if the texture is not too strong and more diffraction lines with different *hkl* can be measured.

The diffraction pattern obtained in this way can provide different information on the crystal structure, phase composition, and microstructure of the sample investigated.

- Positions of the diffraction peaks allow determination of the lattice parameters that are not only basic structural parameters, but they can be related to possible nonstoichiometry, residual stresses, some lattice defects.
- Phase analysis can be performed by comparison with some structural database or Powder Diffraction File.
- Integrated intensities of the diffraction peaks are directly connected to the crystal structure *via* atomic coordinates.
- XRD line broadening is related to small crystallite size and/or microstrain and can be roughly evaluated simply by the modified Williamson–Hall (WH) plot (integral breadth of the diffraction profile β *vs* $\sin\theta$, if the reciprocal space units $1/d$ are used, d is the interplanar spacing and θ is the diffraction angle).

The WH plot is often useful for visualization of the line-broadening effects including their anisotropy. The quantitative evaluation may be complicated by the strong and not too realistic assumptions as the pure summation of crystallite size and microstrain effects (based on the Cauchy distributions of both components). The total XRD pattern fitting based on fundamental approach is preferred. However, in many cases, only a few peaks are available or it may not be easy to build a realistic model including correctly all the necessary microstructural features, and then the WH plot can be useful. It can also be used as the first approximation for estimation of crystallite size and microstrain. Commonly used relation can be modified in order to reduce the errors due to the above approximation, for example as follows:

$$\beta_{hkl}^{\kappa} = K/D_{hkl} + L(4e_{hkl}\sin\theta/\lambda)^{q} \qquad [1]$$

The parameters κ, K, L, and q depend on the considered analytical approximation and relation of importance of both effects.[18] Surprisingly often, different authors simply neglect the second term on the right side of Eq. [1] and determine crystallite size just from a single peak by using the Scherrer equation (basically, the first term on the right side of 1). This is a wrong way unless independent information on microstrain indicates its zero or negligible value, which is usually impossible.

It should be noted here that all the mentioned information—lattice parameters, texture indices, microstrain, and crystallite size—can be contained in a single powder-diffraction pattern and possibly also for each phase, if the sample is multiphase. These parameters can be obtained by separate analysis of a set of individual peaks. However, in the last years, the Rietveld-like approach, total powder pattern fitting has become very popular and often when the diffraction lines are significantly overlapped even inevitable. The programs available can be divided into several groups, as follows, according their main focus:

- Programs for crystal structure refinement like FULLPROF,[19] GSAS,[20] or others. They include

microstructural features such as texture and profile broadening by different phenomenological models that are quite flexible (allow for example for broadening anisotropy). They are written primarily for conventional analysis of powders and symmetric scans. They are widely used also for phase analysis and also sometimes for crystallite size determination.
- Programs focused on the determination of parameters of real structure like crystallite size and its distribution, and dislocation densities, as for example Pm2k[21] or Mfit.[22] They do not allow crystal structure refinement and do not include the effects of texture and residual stresses. They are also written primarily for symmetric scans.
- Programs for combined analysis including asymmetric scans (see below) and effects of texture and stresses, which are suitable for thin films. The program MAUD is the only suitable program.[23,24] However, this program has not included the analysis of dislocations.

Of course, all the programs are under continuous development and try to include more and more features. Our software published recently[25] combines some of the algorithms from the second and some of the features of the third group.

B. *Parallel Beam Geometry (PB), Asymmetric 2θ Scan*

Since for the symmetric scan, the penetration depth is quite high and varying significantly with the diffraction angle, for thin films, in particular very thin layers, the detector scan (2θ scan) taken at fixed and low angle of incidence γ is preferred. This scan can provide in principle similar kind of information as the BB symmetric scan, but each diffraction profile *hkl* is related to the planes differently inclined to the surface ($\psi = \theta - \gamma$). Therefore, a low-angle segment of the pattern may be used only for a rough estimation of texture, if that is not extremely strong. The main advantage of the PB geometry is insensitivity to the specimen displacement and inclination, which is the main reason for its usage for asymmetric scans.

C. *Other Asymmetric Scans Used for Stress and Texture Evaluation*

In thin films, strong fiber textures are often observed. Then simple methods of texture characterization, simple fast scans, can be applied. First of all, it is the *rocking curve* (called also ω scan) when the detector is fixed at the Bragg position corresponding to the measured (*hkl*) planes and sample is rotated about the gonimeter axis. This scan should show a constant intensity (except the instrumental aberrations) for random distribution of crystallites. An observed possible peak indicates texture and its full width at half of maximum (FWHM) is related to the misorientations of crystallites. If the texture axis is inclined with respect to the surface, then the maximum of the ω scan is shifted from the symmetric Bragg position. FWHM of the rocking curve is a suitable parameter for characterization of fiber textures. In case of general textures, which are not fiber, a single ω scan may not be a good characterization of texture. In any case, the second scan is useful—the φ scan—when the detector is fixed at the Bragg position and rotation is made about the axis perpendicular to the thin-film plane. It must be carried out in asymmetric position, on the planes inclined with respect to the surface. The inclination, *i.e.*, the deviation ψ from the symmetric position, can be set to the angle ω at half-width of the ω scan. Variations of the intensity with φ indicate the presence of some preferred orientation in the plane of the film (lateral orientation and nonfiber texture), for fiber texture the intensity should be constant.

Full measurements of pole figures is recommended if the texture is general and should be well characterized. This requires additional experimental setup (*e.g.*, Eulerian cradle).

Residual stresses can also be evaluated from the peak shifts in symmetric scans, but the shifts can have different reasons. Therefore, the deformation is usually measured in asymmetric positions on differently inclined lattice planes and residual stresses are evaluated by the so-called $\sin^2\psi$-method. This is usually realized with the standard two-circle goniometer and θ–2θ scans are taken for studied (*hkl*) planes at different ψ deviations from the symmetric position. In case of simple equi-axial stress, the measured strain ε is given by the relation

$$\varepsilon = \frac{\Delta d}{d} = \frac{1}{2} s_2^{hkl} \sigma \sin^2 \psi + 2 s_1^{hkl} \sigma \qquad [2]$$

where s_i are the X-ray elastic constants, given for elastically isotropic media as $s_1 = -\frac{\nu}{E}$; $s_2 = \frac{1+\nu}{E}$, where E and ν are the Young modulus and Poisson ration, respectively. For elastically anisotropic medium, they are dependent on the grain-interaction model and single-crystal elastic constants s_{ij} or c_{ij}. Corresponding relations can be found in the literature.[26] In order to apply relation [2], some range of ψ inclinations must be available, which may be a problem for highly textured films.

The asymmetric detector (see Section II–B) scan in parallel beam geometry can be used for stress analysis if different diffraction planes are combined for the $\sin^2\psi$ plot. This can be complicated by significant elastic anisotropy.

In general, the ε *vs* $\sin^2\psi$ plot can be curved due to the stress gradients, split for positive and negative values of ψ due to triple-axis stress, or can be completely nonlinear due to the texture. A combination of the effects is, of course, possible. Some of the problems (like triple-axis stress) can be solved quite easily, and others are more complicated.[27–30]

In this article, we consider all the above methods as *routine* XRD methods for thin-film analysis. For the studies of stresses and preferred orientation, we used also a setup with the Eulerian cradle allowing inclinations of the specimen on the axis lying in the diffraction plane. Even though it is also a quite common method, in general, it is used much less for the thin-film analysis,

and we have not included it in a short review of routine methods. On more general approach for studies of texture and stresses, we should mention, for example, References 31 through 33 or recent monographies.[34,35]

III. EXPERIMENTAL CONDITIONS

A. *ZnO Thin Films*

ZnO films were fabricated by PLD using a frequency-quadrupled Nd:YAG pulsed laser (λ = 266 nm, τ = 6 ns, f = 10 Hz, pulse energy of 90 mJ). The experiments were performed in a stainless steel vacuum chamber evacuated by oil-free turbomolecular pumping to a base pressure of 2×10^{-4} Pa. An ultra-high purity ZnO ceramic target was ablated using a laser fluence of 2.8 J cm^{-2}. The films were deposited in oxygen atmosphere at a pressure of 10 Pa on polished c-sapphire (0001), MgO (100), and fused silica (FS) substrates at a substrate temperature of T_s = 573 K (300 °C). The target-to-substrate distance was 55 mm. The substrates were baked out in vacuum at 1223 K (950 °C) before the depositions in an attempt to remove surface contamination. The ZnO thin films were annealed *in situ* at T_s = 1023 K (750 °C) in a 10-Pa oxygen atmosphere after the deposition. The films were studied by optical methods, scanning electron microscopy, and positron annihilation spectroscopy (PAS). For more details on the studies, see Reference 17 and Introduction above.

B. *XRD Measurements*

XRD experiments were performed by using X'Pert Pro and X'Pert materials research diffraction (MRD) powder diffractometers (PANalytical B.V, Almelo, the Netherlands) in conventional parafocusing Bragg–Brentano (θ–2θ) geometry with automatic divergence and antiscatter slits. Glancing-angle incidence (γ = 0.35 deg and γ = 0.5 deg), parallel beam arrangement with Goebel mirror in the incident beam, and parallel plate collimator and monochromator in the diffracted beam, respectively, were used as well. The symmetric Bragg–Brentano scans were recorded with the aid of fast linear detector PIXcel, and in the parallel beam geometry, proportional gas detectors were used. The third kind of measurements was performed on the MRD diffractometer equipped with polycapillary and Eulerian cradle for texture characterization and all the measurements of asymmetric reflections. A parallel plate collimator and secondary graphite monochromator were placed in the diffracted beam. CuKα radiation was used in all cases.

IV. RESULTS

A. *Standard Analysis*

The film thickness was measured by several methods. X-ray reflectivity curves are shown in Figure 1. The obtained values of 81, 75, and 41 nm for MgO, fused silica, and sapphire substrates, respectively, agreed well with measurements by optical spectroscopy and PAS.[17]

Since all the ZnO films were very thin, 2θ scans were measured with the glancing angle parallel beam geometry (angle of incidence γ = 0.35 deg) at first. The scans for films deposited on all three substrates are plotted in Figure 2. The 002** diffraction peak is quite high for all the three films, which could indicate a *c*-axis orientation. Another visible stronger peak is 103. However, 2θ scan is not very appropriate for texture characterization, as noted in Section II–B. Hence, symmetric θ–2θ scans were also measured. The one obtained for the film on amorphous fused silica is shown also in Figure 3. Strong 002 peak supports the conclusion on the strong (0001) preferred grain orientation; however, the other peaks including the fourth order 004 are hardly visible since the thickness of the film was small. Three orders of 001 reflection are shown in three segments also for the film on MgO. Very narrow spurious peaks are artifacts by the substrate. The substrate peaks were avoided in the measurement. No signal from the film at all except a very weak 002 peak was observed for the sapphire substrate (not shown).

**In this article, 4-index notation is used for hexagonal planes, but 3-index notation for the diffraction lines is used commonly in powder diffraction.

The half-widths (FWHMs) of the ZnO 002 rocking curves (ω scans) of the film on MgO and FS substrates were 1.2 and 10 deg, respectively (Figure 4). This indicates that the mosaic spread of planes parallel to the surface (their different inclination to the surface) is relatively small for the films grown on crystalline substrate, and it is much higher for the film grown on FS substrate.

Simplified line broadening analysis was performed on the data obtained from symmetrical θ–2θ scans after the correction on instrumental broadening (LaB_6 standard) with the aid of the modified Williamson-Hall plot.[1]

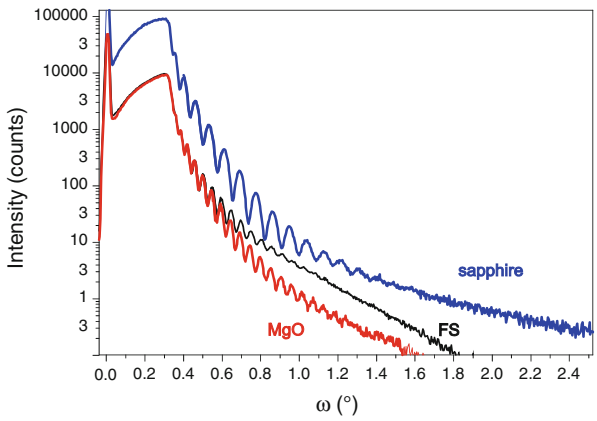

Fig. 1—X-ray reflectivity curves: upper for ZnO on sapphire (0001), middle ZnO on fused silica, bottom ZnO on MgO (100). Slower oscillations for ZnO on sapphire correspond to smaller film thickness.

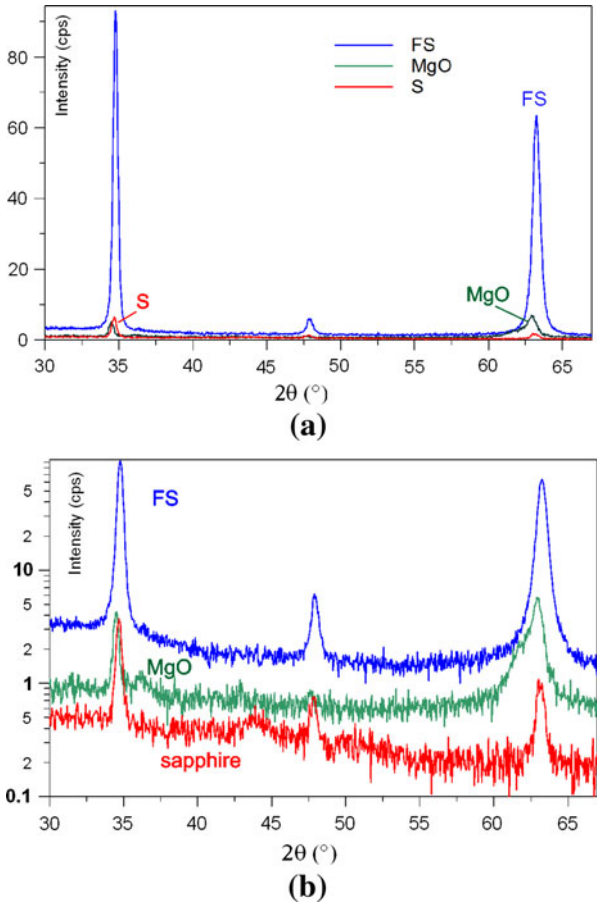

Fig. 2—XRD patterns (intensity in counts per second) of ZnO films deposited on c-sapphire (0001) substrate (bottom thick red curve), on MgO (100) (thin middle green curve) and fused silica (upper thick blue curve). The patterns were taken in the parallel beam glancing-angle geometry with the angle of incidence $\gamma = 0.35$ deg: (*a*) in linear scale and (*b*) in logarithmic scale where the scans were are also scaled in order to separate them on the intensity scale.

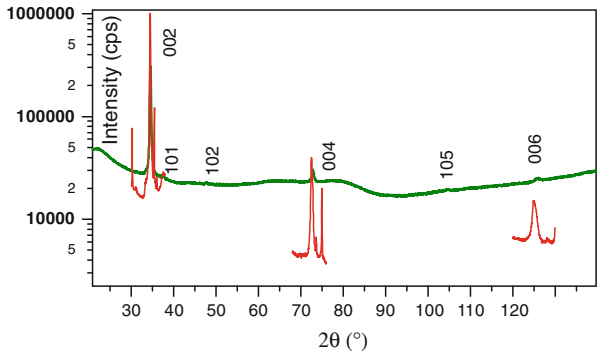

Fig. 3—Symmetric Bragg–Brentano θ–2θ scans for ZnO on fused silica (FS) (continuous green line) and three measured segments (red line) for ZnO on MgO. These measurements were performed with PANalytical MPD and PixCel linear position sensitive detector.

Unfortunately, only three orders of 001 peaks in maximum were available. The mean ZnO crystallite size (D) was estimated to 49 nm and 32 nm for MgO and FS

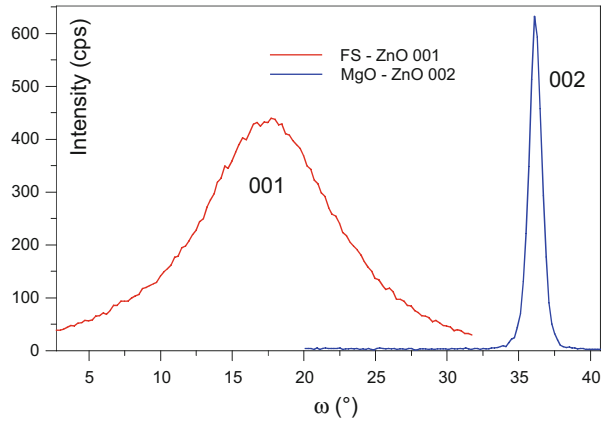

Fig. 4—ω scan for ZnO on FS—reflection 001 and on MgO (100)—reflection 002. The second-order reflection for the film on FS was very weak. On the other hand, higher diffraction angles put lower limits on ω range.

substrates, respectively. Microstrains e of about 0.12 pct contributed to the diffraction line broadening in all cases significantly.

In the following text, a more detailed study of the films investigated is presented.

B. *ZnO on MgO (100)*

1. *Texture*

None of the above measurements is sufficient for structural thin-film characterization, in particular for the growth on single-crystalline substrates. In this case, rather two-dimensional or three-dimensional diffraction pictures of reciprocal space would be desirable. Therefore, further measurements were performed in asymmetric geometry with the Eulerian cradle and polycapillary optics. This only allowed finding of dominant structural characteristic features of the films on the individual substrates. The most complete measurements could be carried out for ZnO film on MgO substrate and also on fused silica because of higher thickness than for the film on sapphire. In addition to ω scans, the φ scans were recorded. These scans must be recorded in an asymmetric position. However, in this case of rather narrow rocking curves, only slight inclinations with respect to the symmetric positions would be possible, and because of limited instrumental resolution, no reasonable information can be obtained in this way. Hence, some information could only be obtained for ZnO on fused silica where the φ scans were constant and indicated fiber texture in these films. Otherwise, asymmetric peaks (*hkil* corresponding to other planes than those with preferred orientation parallel to the surface, *i.e.*, 000*l* in this case) must be scanned at nonzero ψ angles. Of course, full pole figures can be measured as well, but for very strong texture, the measurement steps must be taken very small, and whole measurement may be time consuming. It is preferred to start measurements with a few "smart" scans.

In these measurements, important differences could be found for the three studied substrates. For ZnO on fused silica, the φ scans were also constant. The situation was very different for MgO (100) substrate.

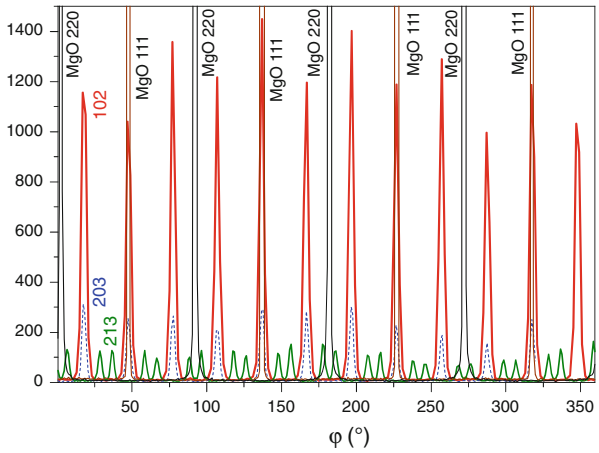

Fig. 5—φ scans of the asymmetric reflections of ZnO film deposited on MgO (100)–102 peak (ψ = 42.8 deg, thick red curve, high peaks), 203 peak (ψ = 51 deg, thin dashed blue curve, small peaks), and 213 peak (ψ = 58.5 deg, thick green curve, small peaks). For comparison, the scans for MgO substrate are also shown—220 peak (ψ = 45 deg, thin black curve, highest labeled peaks), 111 peak (ψ = 54.7 deg, thin brown curve, highest labeled peaks).

The φ scans measured for several asymmetric diffraction planes clearly show periodic maxima (Figure 5). This indicates strong in-plane preferred orientation of grains and local epitaxy. For ($h0\bar{h}1$) lattice planes, in total 12 periodic maxima can be found (Figure 5), while for (*hkil*), their number is 24. In both cases, this is twice higher than it would be derived from the corresponding point symmetry. For better illustration, parts of pole figures are shown in Figure 6. A part of the measured 101 pole figure (in the narrow ψ ring—52 to 68 deg, where the diffracted intensity is significant) in Figure 6(a) shows full symmetry, and therefore, it proves fiber texture for ZnO film on FS substrate. In correspondence with Figure 5, ($10\bar{1}2$) pole figure in Figure 6(b), 12 sharp maxima can be observed. A detail of the ring is shown in Figure 6(c).

This effect can easily be understood if two possible respective orientations of hexagonal basal lattice plane on cubic face are considered (Figure 7). It can be concluded that there are two kinds of domains grown on the MgO (100) substrate. Their respective orientation is also visible from Figure 5 where φ scans for two substrate lattice planes—MgO (111) and (110)—are plotted and show four maxima (there is 4-fold symmetry perpendicular to (100) plane). The positions of MgO 111 peaks coincide with ZnO h0l peaks. In Figure 7, two different orientations of the lattices are shown. Each of the lattices has two kinds of atoms. However, we cannot determine the respective orientation of the individual atoms and nor can we determine lateral shifts. The respective size of the lattices is correct.

2. *Lattice parameters*

θ–2θ scans were recorded for several different asymmetric reflections which were found by the following procedure. The goniometer and the detector were set to the expected diffraction position of the measured *hkl* peak. The angle ψ was set equal to the angle between the (*hkil*) plane and (000*l*) textured plane. Then, a φ scan was performed and the angle φ fixed at one of the above maxima and a short ψ scan in this position taken in order to find and set the intensity maximum. Finally, the θ–2θ scan was performed. This a little cumbersome, but a fast procedure was performed since precise lattice parameters of the measured film were unknown.

All the diffraction peaks measured by this way are shown together with the symmetric scan θ–2θ in Figure 8. In the symmetric scan, only three 001 peaks of ZnO and two h00 peaks of MgO substrate are visible. It can be seen that the MgO substrate peaks are significantly broadened. It seems that the surface layer of the substrate is highly strained. It is difficult to estimate correctly the microstrain from only two peaks taking into account also the necessary gradients, but microstrain values can reach the order of percents in the surface layers of MgO substrate. This can be well understood since the mismatch between atomic distance of the substrate and film is significant. More peaks measured in the way described above allowed determination of the lattice parameters in spite of the fact that the *hk0* peaks could not be measured. The lattice parameters were refined by the software LAPODS[36] as follows: a = 0.3249(1) and c = 0.52087(3) nm. The software uses singular-value decomposition so that the refinement is quite stable (even without *hk0* peaks). It includes also corrections for some aberrations like specimen displacement and specimen transparency. However, in the used parallel beam optics, these effects are negligible. The effect of residual stress is not included. For strongly oriented (0001) ZnO films the stress would cause mainly the change of the c/a ratio. However, the comparison of obtained lattice parameters with the values found in the structure databases like ICSD[37] or PDF-4[38] is questionable because there is quite a large range of published values for both a and c. For example, in the Pearson's Crystal Data,[39] in total 72 records for zincite (*i.e.*, space group $P6_3mc$, no. 186) were found with a = 0.3248 to 0.3253 nm and c = 0.5204 to 0.5213 nm, if some outliers are excluded. The mean values are at a = 0.3249 nm and c = 0.5206 nm. Hence, the measured values are in general agreement with the expected values. The mismatch between cubic MgO and hexagonal ZnO lattices reaches about 8 pct if we compare a_{ZnO} with the square diagonal of MgO lattice—0.2981 nm (measured value, see Figure 7). Residual stress could be estimated from the differences between the c/a ratio obtained for the film and the corresponding powder. Unfortunately, we could not get the free-standing film or powder and because of large spread of database values and uncertainty, which one should be used as a reference and is the only way was to try to measure the strain (and determine the residual stress) directly (see below).

3. *Line broadening*

In order to study strains and crystallite size, the line-broadening analysis (in minimum, the WH plot) should be applied. It must be noted that the used polycapillary parallel beam geometry is extremely unfavorable for such an analysis because of poor resolution. On the

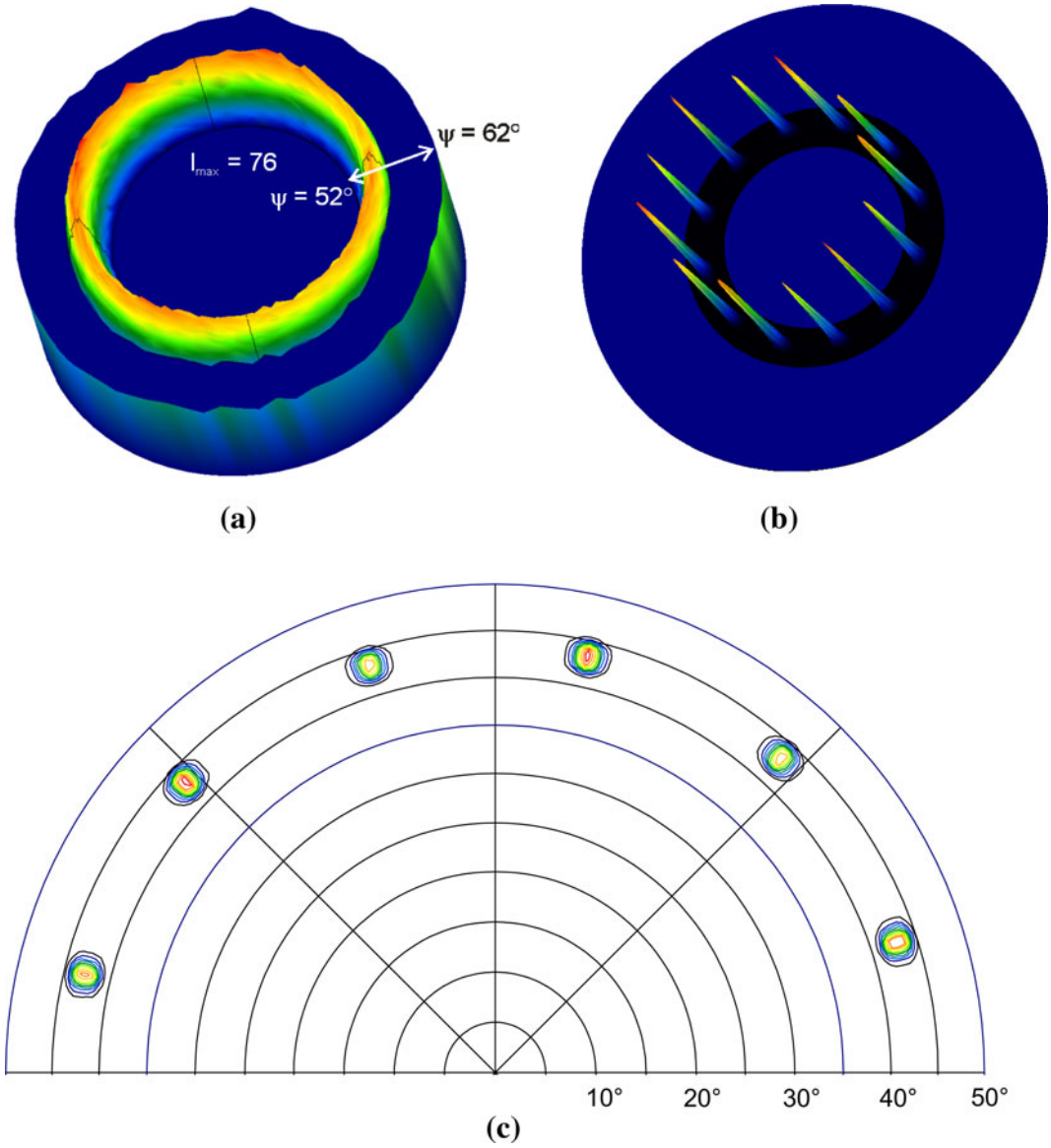

Fig. 6—(*a*) A ring of the (101) pole figure of ZnO film on fused silica showing in-plane isotropy, in the 2.5D representation. (*b*) A ring of the (102) pole figure of ZnO film on MgO (100), in the 2.5D representation. (*c*) Detail of the (102) pole figure of ZnO film on MgO (100) in contour plot.

other hand, it is insensitive to specimen inclinations, and for the studied films, the measured widths were still at least 1.5 to 6 times larger than the instrumental broadening. More difficult situation is for low diffraction angles where the ratio of instrumental and physical broadening is higher. The instrumental broadening was measured on LaB_6a NIST standard, and it was proved that the broadening in the used parallel beam geometry is nearly independent of the ψ inclinations. The measured integral breadths were corrected by the method of the Voigt function. The size–strain analysis was performed on three orders of peaks 00*l*, 002-004-006 and gave values a little different from the Bragg–Brentano geometry (see Section IV–A), $D = 35$ nm and $e = 0.14$ pct (these absolute values, in particular of D, are probably less accurate because of the above reasons). There are no more diffraction lines available with the diffraction vectors oriented perpendicular to the film plane. However, a combined WH plot can be constructed from the both symmetric and asymmetric peaks measured (Figure 8), which can give us an overall picture even though different orientation of corresponding diffraction vectors. This is shown in Figure 9. A large spread of values can be seen on the plot. The lower straight line corresponds to the 00*l* diffractions. For all the other points, actually three parameters should be taken into account: crystallographic direction, dependence on the diffraction vector (sin θ), and the dependence on the lattice plane inclination with respect to the film surface (ψ). The upper straight line on the figure was fitted to the points corresponding to the planes with higher value of ψ (in the interval about 60 to 80 deg) and, hence, similar orientations of the diffraction vectors. A modified WH plot would give the values of 0.28 pct and 39 nm for

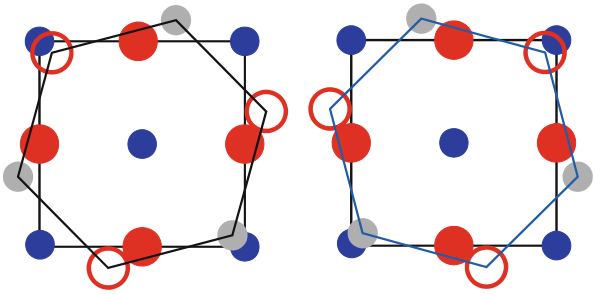

Fig. 7—Schematic picture of two lattice planes—MgO (100) substrate and ZnO basal plane (0001), each with two kinds of atoms in two probable respective rotations (lateral shifts cannot be determined from XRD). For ZnO planes, there are two kinds of either Zn or O atoms with two different heights above the MgO plane differing in 0.5 Å. Dark blue full small circles—Mg atoms, gray small full circles—Zn atoms, larger full red circles—O atoms in MgO, large open red circles—O in ZnO. However, the respective orientation of atoms cannot be determined from the experiment. Therefore, they also can be exchanged in the lattice. The picture should show only the respective orientation of the lattices.

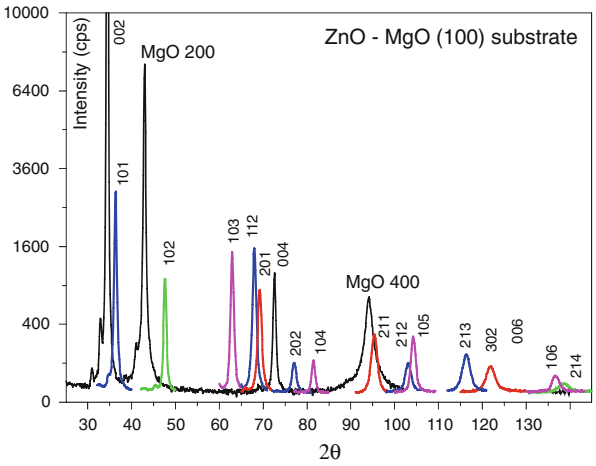

Fig. 8—Diffraction peaks of ZnO layer on MgO (100) substrate obtained in symmetric θ–2θ scan (thin black curve showing 002, 004, 006 ZnO peaks, and MgO broad peaks) and symmetric θ–2θ scans taken for the specimen inclined by different angles ψ with respect to the diffraction plane. The set of angles is the following (for asymmetric reflections) in pairs (hkl)-ψ: 101 to 61.6, 102 to 42.8, 103 to 31.7, 112 to 58, 201 to 74.8, 202 to 61.6, 104 to 24.8, 211 to 78.45, 212 to 67.8, 105 to 20.3, 213 to 58.5, 302 to 70.8, 106 to 17.14, and 214 to 50.74 deg.

microstrain and crystallite size, respectively. Measurements for these highly inclined lattice planes is actually performed in the direction closer to the lateral one and if there is crystallite size anisotropy as for example columnar crystallites, this should be visible on the difference between the intercepts of the above straight lines. However, this is not the case. The estimated crystallite size is somewhat smaller than the film thickness (to be compared with results for 00l diffraction peaks), and it is in quite good agreement with the SEM results showing a wide range of lateral grain size in the range of 30 to 100 nm[17] (to be compared more with the results for inclined planes, upper straight line in Figure 9). Significant differences can be found in microstrain. We have also tried to investigate

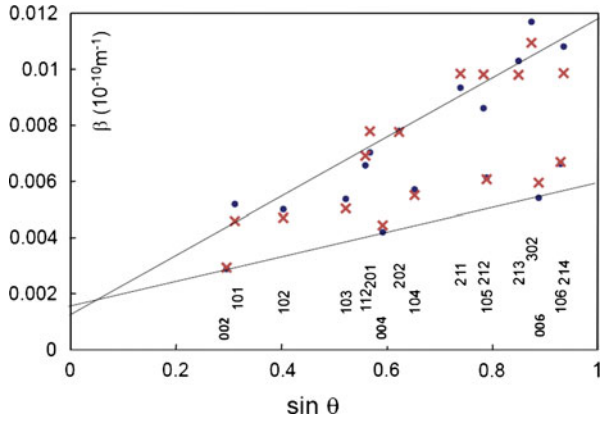

Fig. 9—Williamson–Hall plot for combined symmetric (001) and asymmetric peaks for ZnO film on MgO substrate (dots). Indices of individual reflections are shown. The bottom and upper lines correspond to linear fits to reflections corresponding to basal symmetric planes and asymmetric planes with ψ inclinations to the surface within the interval 60 to 80 deg, respectively. The crosses correspond to the calculations according to the simple model described in the text.

line broadening anisotropy and to find functional dependence of line broadening on θ and ψ angles in order to reveal any significant correlation between the anisotropy and lattice plane inclination. Finally, relatively good fit (Figure 9) was obtained by assumption of summation of ψ-independent size and strain terms as in the WH plot and ψ-dependent both terms as follows:

$$\beta_{hkl} = K/D_{hkl} + (K/D_{hkl})f(\psi) + 4e_{hkl}\sin\theta/\lambda + (4e_{hkl}\sin\theta/\lambda)f(\psi) \quad [3]$$

Different functions f for the ψ-dependence of line broadening were tested, but clearly the best fits were obtained with the function $\sin^2\psi$ multiplying the strain term as an analogy to the residual stress method. The calculated values are shown by crosses in Figure 9. This is nothing more than only a very approximate phenomenological estimation, but we believe that the ψ-dependence is described quite well. The nonlinear optimization always leads to zero ψ-dependence of the crystallite size term as it follows also from the plot. Hence, the anisotropy is completely given by the microstrain.

4. *Residual stress*

In order to reveal possible stresses, only a short range of ψ-inclinations could be used. Therefore, detailed θ–2θ scans were taken around the spots of asymmetric reflections (ψ range of 3 deg only). The map of a reciprocal point in plot 2θ *vs* ψ is shown in Figure 10. It can be seen that the spot is inclined with respect to the horizontal line in the way that the intensity is increasing with both 2θ and ψ angles. This would clearly indicate compressive stress. It is quite difficult to apply the $\sin^2\psi$ method because of very narrow ψ range available. Anyway, for quantitative estimation the $\Delta d/d$ *vs* $\sin^2\psi$ plots were evaluated for several diffraction peaks hkl

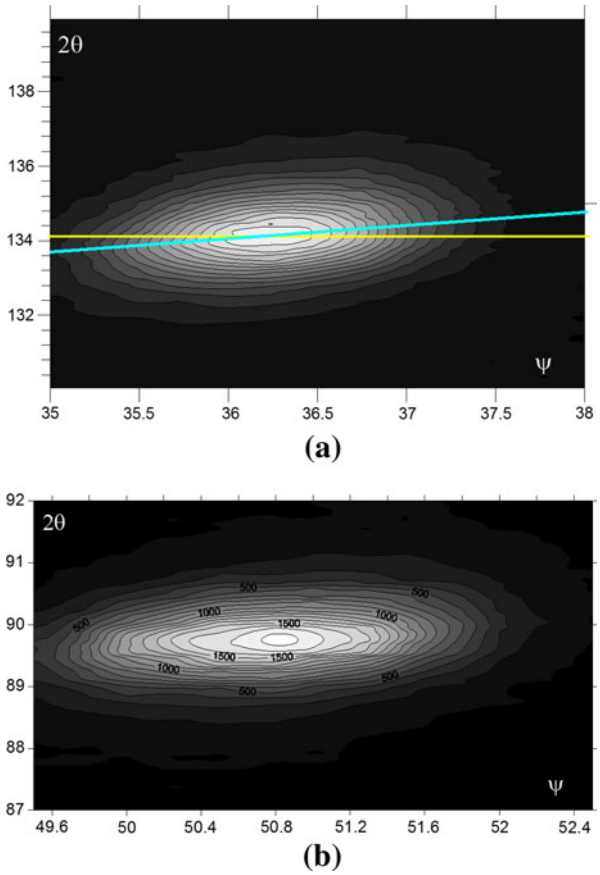

Fig. 10—Maps of the diffraction spots 205 (*a*) and 203 (*b*) of ZnO film on MgO(100) in plots of 2θ *vs* ψ.

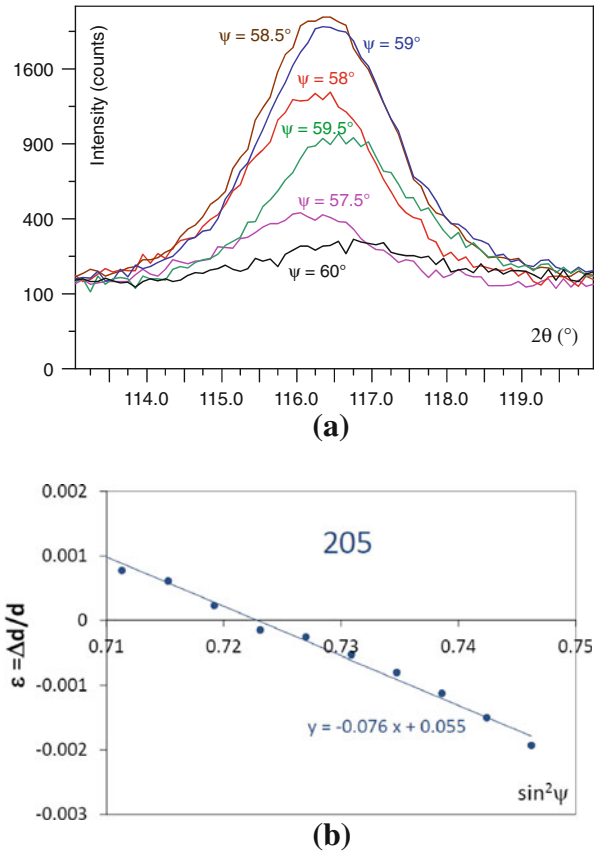

Fig. 11—Diffraction peak shifts (*a*) and application of $\sin^2\psi$ method to 205 diffraction peak in narrow ψ range (*b*). Parameters of linear fit are shown. As reference *d* values, the values from PDF-4+ database for ZnO were taken.

(Figure 11, for example of 205 diffraction peak and huge peak shifts). All the scans confirmed the presence of compressive residual stress, and all the $\sin^2\psi$ dependences were approximately linear so that relation [2] was used for the stress estimation. By using the literature values of elastic modulae,[40] $E = 123$ GPa, $\nu = 0.36$, we obtained extremely high stress of -14 ± 1 GPa (the error is statistical). It is questionable if the application of formula [2] in case of very strong texture is well justified. The results (slopes of $\Delta d/d$ *vs* $\sin^2\psi$ plots) agreed well for all the measured peaks at different ψ-inclinations. However, if we compare the values of *a, c* lattice parameters (or ratio c/a) with any of the above data found in structure databases or respective peak shifts for the other two samples (see below), the obtained stress value could be estimated to –0.4 GPa only. Therefore, the application of $\sin^2\psi$ method for quantitative residual stress determination seems to be incorrect in this case.

5. *ZnO on fused silica and sapphire (001)*

Combined WH plot constructed for the lattice planes differently inclined to the surface for the ZnO film on FS is shown in Figure 12. However, in this case high-angle peaks were not detectable so that only 10 peaks instead of 17 (as for MgO) were analyzed. Unfortunately, only two orders of 001 peaks were available and gave the values $D = 35$ nm, $e = 0.12$ pct. Unlike the MgO substrate, for the planes with higher inclinations

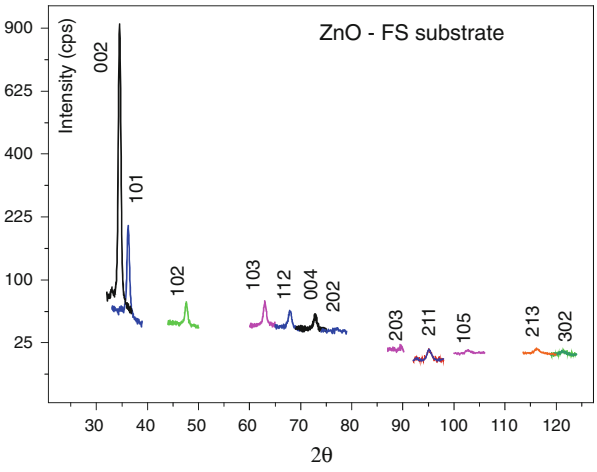

Fig. 12—Diffraction peaks of ZnO layer on fused silica substrate obtained in symmetric θ–2θ scan (001 peaks) and symmetric θ–2θ scans recorded for the specimen inclined by different angles ψ with respect to the diffraction plane (Fig. 9).

($\psi = 60$ to 80 deg), some differences were found for both crystallite size and strain ($D = 29$ nm, $e = 0.15$ deg; Figure 13). It should be noted that the peaks are quite weak (Figure 12) and the errors are in

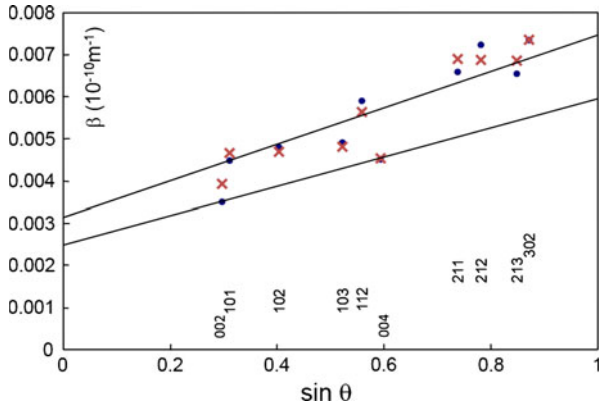

Fig. 13—Williamson–Hall plot for combined symmetric (001) and asymmetric peaks for ZnO film on fused silica (dots). Indices of individual reflections are shown. The bottom and upper lines correspond to linear fits to reflections of basal symmetric planes and asymmetric planes with ψ inclinations to the surface within the interval 60 to 80 deg, respectively. The crosses correspond to the calculations according to the procedure described in the text.

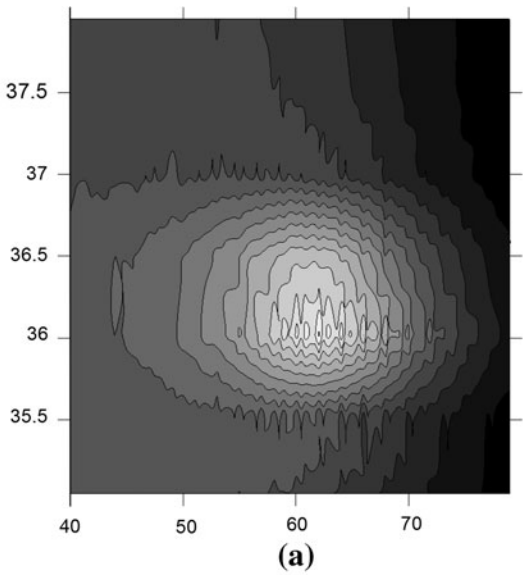

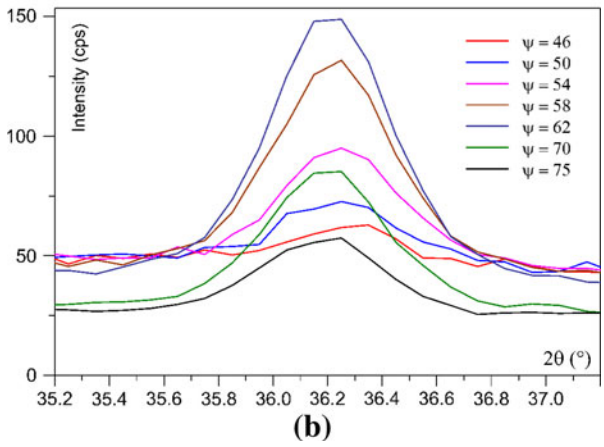

Fig. 14—(*a*) Map of the diffraction spots 110 of ZnO film on FS in plot of 2θ *vs* ψ. (*b*) XRD line profile of ZnO 110 (on FS) for different ψ inclinations from ψ = 46 deg to ψ = 75 deg.

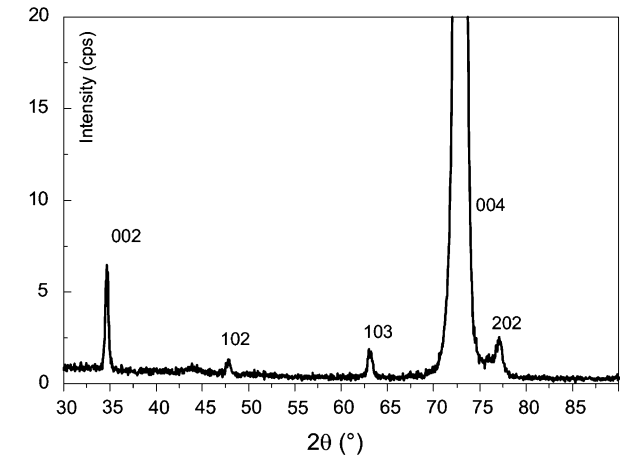

Fig. 15—XRD pattern of ZnO film deposited on sapphire (0001) in extended range with respect to Fig. 2. The pattern was taken in the parallel glancing-angle geometry with the angle of incidence γ = 0.35 deg.

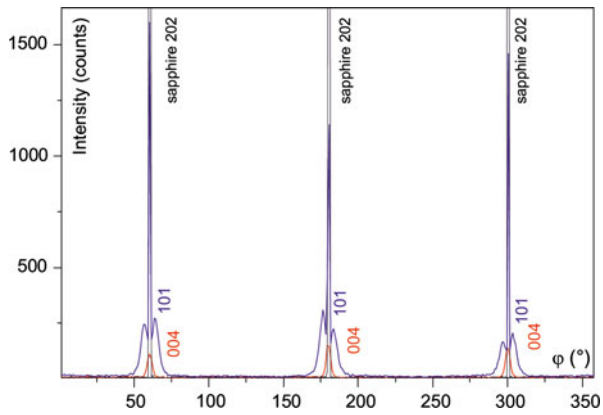

Fig. 16—φ scans of the asymmetric reflections of ZnO film deposited on sapphire (0001) – 004 peak (ψ = 42.8 deg, thick red curve, small peaks), 101 peak (ψ = 37.08 deg, blue curve, high peaks). For comparison, the scan for sapphire substrate is also shown −202 peak (ψ = 72.36 deg, thin black curve).

principle larger than in the case of MgO substrate. However, the agreement with the SEM results (lateral grain size in the range of 20 to 50 nm,[17]) is quite good. Microstrain values for 00*l* diffraction lines, *i.e.*, in the direction perpendicular to the surface, are similar to those for ZnO on MgO, but for the diffraction vector inclined to the lateral direction, the microstrain is much higher for the single crystalline substrate. This is in agreement with the SPIS measurements (See Section I and Reference 17), and it is explained by higher density of misfit dislocations compensating a large mismatch between ZnO and MgO lattices.

The lattice parameters were refined as follows: a = 0.32569 (7) and c = 0.5195 (2) nm. The lattice cell is slightly expanded in a and contracted in c, in comparison with the film on MgO substrate, or it may be better written than the film on MgO substrate is contracted in a and expanded in c directions, as this is

also in agreement with the stress estimated from detailed mapping of peak shifts similar to MgO substrate (Figure 14). In this case, however, the shifts were opposite and correspond to the tensile stress of about (0.9 ± 0.13) GPa, if estimated from the $\sin^2\psi$ plots, and to +0.5 GPa if estimated from the respective shifts of 001 peaks (see Section IV–B–1).

Unfortunately, the method could not be well applied for sapphire substrate since the film was significantly thinner, and not many peaks could be measured. It

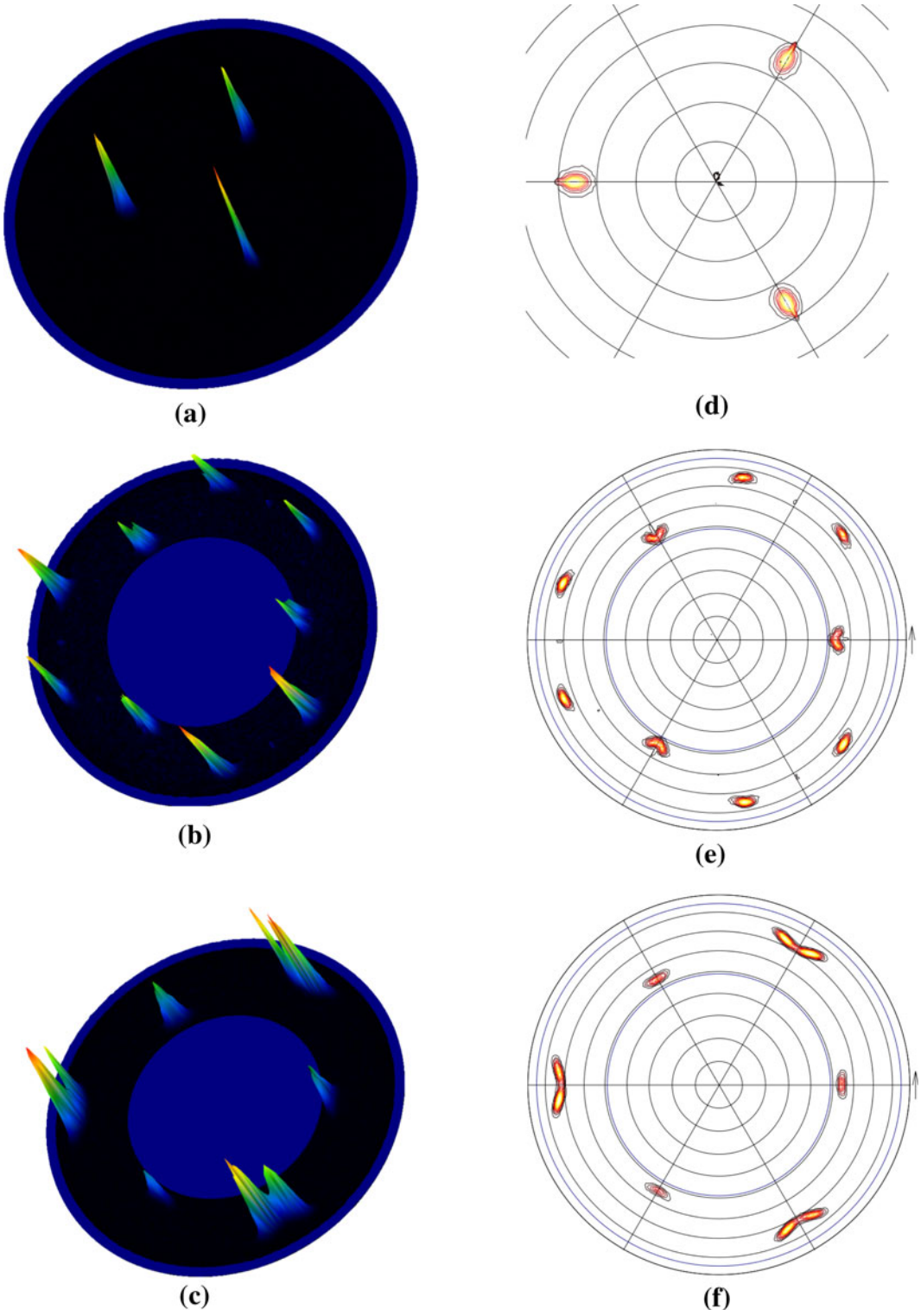

Fig. 17—Pole figures measured for reflections 002 (*a*, *d*), 102 (*b*, *e*), and 110 (*c*, *f*) of ZnO film on sapphire (0001) in 2.5D representation (a through c) and as contour plots (d through f). In the latter plots, the regular black circles are separated by 10 deg.

might even seem that there were no reflections at all since in the symmetric scan only very weak 002 ZnO peak and substrate peaks were detected. In the glancing angle detector scan (Figure 2), weak peaks 002, 102, 103 could be observed. Usually, the main features of XRD pattern, from the point of view of phase and texture analysis, can be found in the low-angle region, but it appeared that this was not the case. It was helpful to extend the scan to higher diffraction angles (Figure 15) where a strong 004 peak appeared. However, this was not in symmetric mode. The (000*l*) planes were not parallel to the surface as one could expect for the reported epitaxy on sapphire (000*l*).[41,42] This means that there were no simple planes of the film oriented preferentially parallel to the substrate (000*l*) planes. In this case, φ scans of asymmetric reflections 002 and 004 were taken at $\psi = 35.7$ deg, and three maxima were observed clearly. They well fit with the 101 maxima of sapphire substrate. The φ scan of 101 peak ($\psi = 37.8$ deg) was also possible and showed maxima at the same positions (Figure 16). However, the maxima have satellites on both sides, which probably correspond to misoriented domains. It may be concluded that also for sapphire substrate, the main feature of ZnO films was local epitaxy, although not determined by basal lattice planes. The pole figures measured on 002, 110, and 102 peaks are shown in Figure 17 and indicate 3-fold symmetry, but several maxima are sometimes split due to domains. The above procedure of combination of several asymmetric planes was not too efficient since only a few low-angle peaks were accessible. Finally, we could observe three orders of 001 peaks in asymmetric position and applied the WH analysis giving the following values: $D = 31$ nm, $e = 0.2$ pct. The values correspond to the planes inclined by and angle 35.7 deg with respect to the surface, which must be taken into account in comparison with the above results. For asymmetric peak 004, a detailed mapping of peak shifts with ψ-inclinations was performed as above. However, unlike MgO and FS substrates, in this case no shifts were observed, which indicates absence of residual stresses (Figure 18).

It looks like some general high-index plane of the film is parallel to the (0001) plane of the substrate and also that different domains are present in the film. In general, it is possible that slightly distorted wurtzite ZnO structure with the *c*-axis inclined by ~36 deg with respect to the sapphire (0001) plane enables better matching of both ZnO and Al_2O_3 lattices, which have a large misfit (18 deg). However, it seems that this appears only for very thin films. The plane that is the closest to the orientation parallel to the surface is ($20\bar{2}5$). This would correspond partially to two of the pole figures, but agreement is not complete and a more detailed analysis of this film orientation still should be done. Preparation of these films with different thickness is planned.

6. *Final Remarks*

Microstructure of nanocrystalline ZnO thin films was studied by a combination of different XRD scans that revealed strong preferred orientation, local epitaxy on single crystalline substrates, and significant different residual stresses. The analysis of such films cannot be performed by the Rietveld-like programs (2.1), and therefore, simple methods like the Williamson–Hall plot were used for the evaluation of a set of diffraction peaks recorded at suitable angles as in the case of single crystals.

The results obtained for residual stresses in all the films by the inclinations of the sample are actually in qualitative agreement with peak shifts observed in BB and PB symmetric and asymmetric scans (Figure 2). Large respective peak shifts for the films on MgO and FS are visible in Figure 3. The differences in peak positions are larger than 1 deg at high diffraction angles but still do not correspond to enormous compressive stresses (larger than 10 GPa for MgO substrate) determined by application of conventional $\sin^2\psi$ method in narrow range of ψ with nonzero intensity. Therefore, we assume that the application of the simple $\sin^2\psi$ method for quantitative residual stress evaluation in these cases seems to be incorrect, and the measurable range of ψ is too narrow to decide if this simple method can be used.

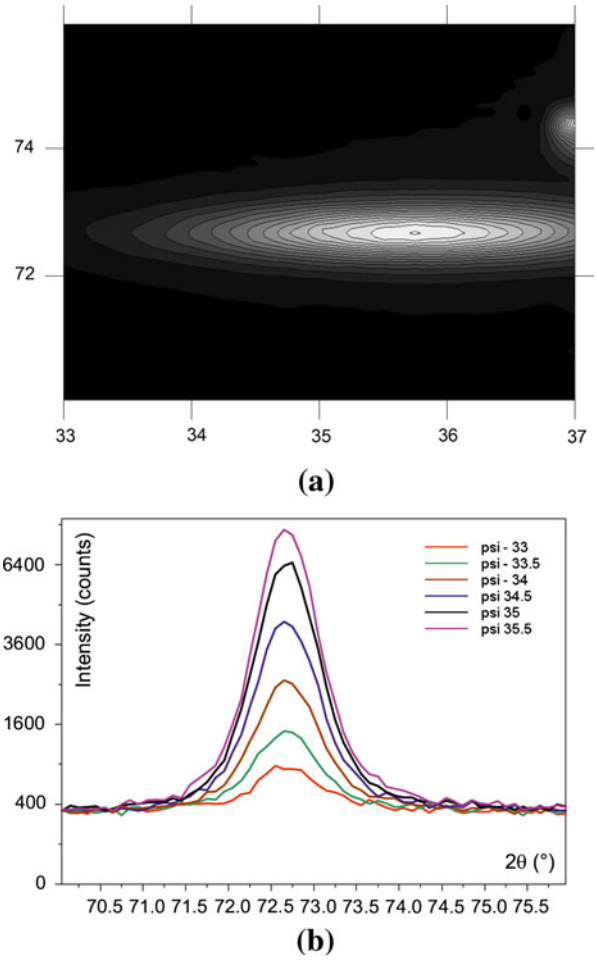

Fig. 18—(*a*) Map of the diffraction spots 004 of ZnO film on sapphire in plot of 2θ *vs* Ψ. (*b*) XRD line profile of ZnO 004 for different ψ inclinations from $\psi = 33$ deg to $\psi = 35.5$ deg.

V. SUMMARY

XRD characterization of thin films by simple conventional methods can be very useful, but sometimes it is also insufficient and basic microstructural features of the films often fundamental for their properties may remain hidden. This is especially true for the films with strong preferred orientation. Three types of films were selected for the analysis.

ZnO films deposited on MgO (100) and sapphire (0001) single crystalline substrates and amorphous fused silica showed different kinds of preferred orientation and residual stresses. While the texture of the film deposited on fused silica was of fiber type, φ scans on asymmetric reflections revealed the presence of local epitaxy in the films deposited on the single-crystalline substrates. There are ZnO hexagonal basal plane (0001) domains of nanocrystalline size on MgO (100) substrate that can have two different orientations. XRD line broadening was analyzed by a combination of different asymmetric reflections scanned at different plane inclinations with respect to the surface. Local epitaxy was found also on sapphire (0001), but this was rather unexpected since basal planes of the ZnO film were not parallel to the film plane. Large residual stresses were found in ZnO films in particular those deposited on MgO (compressive) and fused silica (tensile). No stresses were detected in case of sapphire substrate.

ACKNOWLEDGMENTS

The work is supported by the Grant Agency of the Czech Republic under the numbers P108/11/1539 and P108/11/0958.

REFERENCES

1. A. Jain, P. Sagar, and R.M. Mehra: *Solid State Electron.*, 2006, vol. 50, pp. 1420–24.
2. D.P. Norton: *Mater. Sci. Eng. R*, 2004, vol. 43, pp. 139–247.
3. S.J. Pearton, D.P. Norton, K.I.Y.W. Heo, and T. Steiner: *Progr. Mater. Sci.*, 2005, vol. 50, p. 293.
4. A. Janotti and C.G. Van deWalle: *Rep. Prog. Phys.*, 2009, vol. 72, p. 126501.
5. K. Ellmer, A. Klein, and B. Rech: *Transparent and Conductive Zinc Oxide, Basics and Applications*, Springer Series in Materials Science, vol. 104, Springer, New York, 2008.
6. H. Morkoç and Ü. Özgrür: *Zinc Oxide, Fundamentals, Materials and Device Technology*, Wiley, New York, NY, 2009.
7. J.C. Nie, J.Y. Yang, Y. Piao, H. Li, Y. Sun, Q.M. Xue, C.M. Xiong, R.F. Dou, and Q.Y. Tu: *Appl. Phys. Lett.*, 2008, vol. 93, p. 173104.
8. R. Eason: *Pulsed Laser Deposition of Thin Films. Applications. Led Growth of Functional Materials*, Wiley, Hoboken, NJ, 2007.
9. M. Birkholz: *Thin Film Analysis by X-Ray Scattering*, Wiley, Weinheim, Germany, 2006.
10. C.V. Thomson and R. Carel: *Mater. Sci. Forum*, 1996, vols. 204–206, pp. 83–98.
11. N. Kaiser: *Appl. Optic.*, 2002, vol. 41, pp. 3053–60.
12. Z. Cao: *Thin Film Growth. Physics*, Woodhead Publishing Limited, China, 2001.
13. M. Ohring: *Materials Science of Thin Films*, 2nd ed., Academic Press, Atlanta, GA, 2001.
14. L.B. Freund and S. Suresh: *Thin Film Materials: Stress, Defect Formation and Surface Evolution*, Cambridge University Press, New York, NY, 2009.
15. M. Suchea, S. Christoulakis, M. Katharakis, G. Kiriakidis, N. Katsarakis, and E. Koudoumas: *Appl.Surf. Sci.*, 2007, vol. 253, pp. 8141–45.
16. J.M. Myoung, W.H. Yoon, D.H. Lee, I. Yun, S.H. Bae, and S.Y. Lee: *Jpn. J. Appl. Phys.*, 2002, vol. 41, pp. 28–31.
17. M. Novotny, J. Cizek, R. Kuzel, J. Bulir, J. Lancok, J. Connolly, E. McCarthy, S. Krishnamurthy, and J.P. Mosnier: *J. Phys. D*, 2012, vol. 45 (22), 225101.
18. R. Kužel, R. Černý, V. Valvoda, M. Blomberg, and M. Merisalo: *Thin Solid Films*, 1994, vol. 247, pp. 64–78.
19. J. Rodriguez-Carvajal: *Phys. B*, 1993, vol. 192, p. 55.
20. A.C. Larson and R.B. Von Dreele: "General Structure Analysis System (GSAS)", Los Alamos National Laboratory Report LAUR, 1994, pp. 86–748, http://www.ccp14.ac.uk/solution/gsas/.
21. P. Scardi and M. Leoni: *J. Appl. Crystallogr.*, 2006, vol. 39, pp. 24–31.
22. G. Ribárik, T. Ungár, and J. Gubicza: *J. Appl. Crystallogr.*, 2001, vol. 34, pp. 669–76.
23. L. Lutterotti: *Nucl. Instrum. Methods Phys. Res. B*, 2010, vol. 268, pp. 334–40.
24. L. Lutterotti, D. Chateigner, S. Ferrari, and J. Ricote: *Thin Solid Films*, 2004, vol. 450, pp. 34–41.
25. Z. Matěj, R. Kužel, and L. Nichtová: *Powder Diffr.*, 2010, vol. 25, pp. 125–31.
26. I.C. Noyan and J.B. Cohen: *Residual Stress Measurement by X-Ray Diffraction and Interpretation*, Springer, Berlin, Germany, 1987.
27. M. Klaus, C. Genzel, and H. Holzschuh: *Thin Solid Films*, 2008, vol. 517, pp. 1172–76.
28. H. Behnken and V. Hauk: *Mater. Sci. Eng. A*, 2001, vol. 300, pp. 41–51.
29. A. Kumar, U. Welzel, and E.J. Mittemeijer: *J. Appl. Crystallogr.*, 2006, vol. 39, pp. 633–46.
30. U. Welzel, J. Ligot, P. Lamparter, A.C. Vermeulen, and E.J. Mittemeijer: *J. Appl. Crystallogr.*, 2005, vol. 38, pp. 1–29.
31. C.M. Brakman: *J. Appl. Crystallogr.*, 1983, vol. 16, pp. 325–40.
32. C.M. Brakman: *Acta Crystallogr. A*, 1987, vol. 43, pp. 270–83.
33. M. Barral, J.L. Lebrun, J.M. Sprauel, and G. Maeder: *Metall. Trans. A*, 1987, vol. 18A, pp. 1229–38.
34. D. Chateigner: *Combined Analysis*, Wiley, New York, NY, 2010.
35. V. Randle and O. Engler: *Introduction to Texture Analysis: Macrotexture, Microtexture and Orientation Mapping*, CRC Press, Boca Raton, FL, 2009.
36. C. Dong and J.I. Langford: *J. Appl. Crystallogr.*, 2000, vol. 33, pp. 1127–79.
37. Inorganic Crystal Structure Database, FIZ Karlsruhe, http://www.fiz-karlsruhe.de/icsd.html.
38. Powder Diffraction File, PDF-4, International Centre for Diffraction Data http://www.icdd.com.
39. Pearson's Crystal Data, Crystal Impact, http://www.crystalimpact.com.
40. G.C. Gadzhiev: *High Temp.*, 2003, vol. 41, pp. 778–82.
41. P. Fons, K. Iwata, S. Niki, A. Yamada, and K. Matsubara: *J. Cryst. Growth*, 1999, vols. 201–2, pp. 627–632.
42. Y. Chen, D.M. Bagnall, H.-J. Koh, K.-T. Park, K. Hiraga, Z.-Q. Zhu, and T. Yao: *J. Appl. Phys.*, 1998, vol. 84, p. 3912.